Numerical and Experimental Investigation of Fuel Spray Behaviour in Very High Density Environment Using LES

O. Kaario, T. Hulkkonen, V. Vuorinen, A. Wehrfritz, K. Keskinen, and M. Larmi
Department of Energy Technology, Aalto University, Finland
ossi.kaario@aalto.fi

Abstract

An effective way to increase the specific power from engines is to increase the maximum cylinder pressure. However, this also increases the gas density which has significant effect to the fuel spray evolution. In this study, experimental data from room temperature conditions at gas density of 39 kg/m^3 and at very high gas density of 115 kg/m^3 representing cylinder density at 300bar pressure conditions is compared to fuel spray large eddy simulations (LES). Special attention is put to the analysis of turbulence on local basis but also on a spray-induced volume basis. It is observed that several realistic features that can be seen in experimental sprays could be identified from the simulated fuel sprays. These include local turbulent structures, droplet clustering, and non-symmetric features. The computational model was also able to produce a range of frequencies and small scale structures which are needed from a properly working LES simulation. The spray opening angles as well as the droplet sizes were well captured with the LES model whereas the trend for the spray penetration was somewhat too long. The main reason for this is believed to be the mesh resolution that did not produce quite enough momentum spreading close to the nozzle.

Introduction

The demand for specific power from engines is continuously increasing as the trend is towards smaller size engines with at least the same power as in the original one. One effective way to increase cylinder power is to increase the maximum cylinder pressure. By increasing the cylinder pressure, also the gas density is increasing. However, it is well known that gas density has significant effect to the fuel spray behavior in engines. Typically, when considering global spray parameters, as gas density increases, the spray tip penetration decreases and the opening angle increases [1]. As a consequence, the fuel vapor mixing behavior and the subsequent combustion and emission formation processes are affected by the gas density change. At the Department of Energy Technology in Aalto University, an engine has been developed that is able to operate at 300bar maximum cylinder pressure level [2, 3]. The 300bar cylinder pressure level indicates gas density values of more than 100 kg/m^3. The aim of this research is to analyze the fuel spray behavior in very high 115 kg/m^3 gas density conditions by experimental and numerical methods at room temperature.

Typically, fuel spray studies have been carried out well below 100 kg/m^3 gas densities [4, 5, 6]. In this respect, the currently used gas density of 115 kg/m^3 can be considered to be a significant increase. The 115 kg/m^3 experiments have been carried out in a constant volume bomb at room temperature. The spray tip penetration and the spray opening angle were defined from the experimental results. In addition, validation of the LES model will be done against another experimental data reported by Larmi et al. [6] conducted at gas density of 39 kg/m^3 where also droplet sizes were measured. Therefore, in addition to spray penetration and opening angle in the 39 kg/m^3 conditions, droplet size data will also be used for the numerical model validation.

Large Eddy Simulation (LES) is used in the current study to model the fuel sprays. Similar type of work has been done previously by e.g. Hori et al. [7] who observed strong grid sensitivity that affected especially the spray penetration. Their solution was to select mesh density in a way that gave reasonable comparison with experimental data. Bharadwaj and Rutland [8] showed the effect of direct source term from droplets to the sub-grid turbulent kinetic energy equation in LES gas jet and engine spray simulations. In their simulations, spray tip penetration was over estimated without the source term. Recently, in [9], LES simulation of fuel sprays was carried out in evaporating and non-evaporating conditions. They found it difficult to obtain good agreement between the experimental and simulated spray penetration without modifying the turbulent viscosity. Not modeling the near-nozzle region, Vuorinen et al. [10] showed the effect of droplet Stokes number (St) to the spray shape and penetration in implicit LES. It was shown that small droplets (St<1) follow the flow field and disperse effectively whereas large droplets (St>1) follow more their ballistic trajectories.

The LES model used in this work is a one-equation model for the turbulent kinetic energy and an algebraic model for the dissipation rate of the kinetic energy. Using St number arguments, the current study uses relatively small droplet sizes at the near-nozzle region. The simulation is started at $z \sim 6d_n$, where z is the distance from the geometrical nozzle hole d_n in order to avoid the short intact liquid core region. It is observed that the current LES model produces many features that are visible in experimental sprays including local turbulent structures, droplet clustering, and non-

symmetric features. The LES model is also able to produce droplet sizes and spray opening angles that resembled those observed in experiments. However, the spray penetration is somewhat overpredicted mainly due to mesh resolution close to the nozzle that does not produce enough momentum spreading.

Experimental Methods

Experimental fuel spray measurements were performed with laser based backlight imaging system at pressurized injection test chamber. In the backlight imaging, illumination of images is done with a planar light source. At first, a short duration laser pulse is expanded with lens. While originally green laser light (532 nm) is shot to a fluorescent plate, the light is phase shifted to white light. This is done to get even and planar light to measurements. The light is further smoothed with a milk glass diffusor. Without phase shifting laser light will cause significant laser speckling which will ruin image quality and make detailed image consideration difficult.

The optical access to the injection test chamber was through four windows at different sides. The light source was a pulsed Nd:YAG laser sheet with 532 nm wavelength after second harmonic generator. The images were taken with digital monochrome camera (CCD). Duration of a laser pulse was approximately 5 ns. Due to the short light pulse, most motion of high-velocity fuel spray is frozen and high timing accuracy can be achieved. The measurements were controlled by a computer, which was also used for data acquisition. The resolution of camera was 2048x2048 pixels (four megapixels) with dynamic range of 12 bit (4096 different levels of grey). The optic was Nikon Micro-Nikkor 105mm teleobjective with 25 mm extension tube.

Experiments at gas density of 115 kg/m^3

The test chamber is emulating the physical conditions in diesel engines. However, fuel sprays were non-evaporative and ambient gas density is constant 115 kg/m^3 in the test chamber. Injection pressure is 1000 bar. Maximum variance of injection pressure in the common rail was ±25 bar and maximum variance of ambient gas density was ±0.15 kg/m^3. Ambient gas temperature was 20-25 °C when density of ambient gas was kept constant by varying ambient pressure. The pressurizing gas, nitrogen (N_2), was flowed continuous through the chamber to ensure that chamber is clear of diesel mist before next injection. The injector was solenoid operated common rail injector. Nozzle orifice diameter was 0.34 mm. The cone angle was 156 degrees. The images were captured between 0.915 ms and 2.000 ms after electric start of injection. Some delay from the electric injection signal to fuel jet exit from the nozzle orifice is occurred. This is mainly due to solenoid operation, needle inertia and fluid inertia. Injected fuel is European standard diesel EN590. Density of fuel is 837.3 kg/m^3 (15°C).

Total 466 images was taken and analyzed when spray tip penetration is studied. Total 50 images is taken and analyzed when spray angle was studied. The area of view is approximately 64.8x64.8 mm and dimensions of pixels are approximately 31.6x31.6 μm. Images are analyzed by computer program. Algorithms of computer program are based on difference of light intensity between spray and background.

Experiments at gas density of 39 kg/m^3

The experiments conducted in gas density of 39 kg/m^3 are detailed in Larmi et al. [6]. They were done in a relatively similar manner as detailed above in the general part of the experimental methods –section. The biggest difference compared to the current 115 kg/m^3 gas density experiments is that in the earlier measurements also droplet sizes were measured. In [6] they used special cutters to be able to measure droplet sizes from different radial distances from the spray axis at about 60mm from the nozzle. The droplet sizes we measured from a fully developed spray meaning that they were typically measured after 1ms from the start of injection. The spray tip penetration was analyzed using 20 to 50 images. The spray opening angle was defined using 20 different images. The spray width was defined from a fully developed spray at 62mm from the nozzle.

Tables 1 and 2 summarize the conditions and fuel properties used in the experiments and simulations.

Table 1. Summary of experimental conditions.

Experimental conditions	1	2
Gas density [kg/m^3]	39	115
Nozzle size [mm]	0.37	0.34
Injection pressure [bar]	700	1000

Table 2. Summary of fuel properties.

Density, +15 ºC [kg/m^3]	837
Surface tension [N/m]	0.029
Viscosity, +30 ºC [kg/ms]	0.00269

Numerical model

The LES model used currently is a one-equation model for the sub-grid turbulent kinetic energy k_{sgs} given by

$$\frac{\partial \bar{\rho} k_{sgs}}{\partial t} + \frac{\partial \bar{\rho} \langle u_j \rangle k_{sgs}}{\partial x_j} = -\tau_{sgs,ij} \langle s_{ij} \rangle - c_1 \bar{\rho} \frac{k_{sgs}^{3/2}}{\Delta} + \frac{\partial}{\partial x_j} \left[c_2 \bar{\rho} \Delta \mathrm{k}_{\mathrm{sgs}}^{1/2} \frac{\partial \mathrm{k_{sgs}}}{\partial \mathrm{x_j}} \right] \quad (1)$$

where c_1 and c_2 are model constants with the values of 1 and 0.05, respectively, and Δ is the filter width (characteristic cell size). The values used in this study for the model constants c_1 and c_2, are of similar magnitude than used e.g. in [7] and [11]. The sub-grid rate of strain τ_{sgs} is modelled according to $\tau_{sgs,ij} = -\mu_t \langle s_{ij} \rangle + \delta_{ij} \frac{2}{3} \bar{\rho} k_{sgs}$, where μ_t is the turbulent viscosity, and the deformation tensor is written as $s_{ij} = \frac{1}{2} \left(\frac{\partial u_i}{\partial x_j} + \frac{\partial u_j}{\partial x_i} \right)$. The sub-grid kinetic energy k_{sgs} is used in the turbulent viscosity equation written as $\mu_t = c_2 \bar{\rho} \Delta k_{sgs}^{1/2}$. The sub-grid dissipation rate of the turbulent kinetic energy is computed from $\varepsilon_{sgs} = c_1 k_{sgs}^{3/2} / \Delta$. The advantage of the present model is that it is capable of capturing non-equilibrium effects between production and dissipation of the kinetic energy in the sub-grid scales [7, 11]. Additionally, the current model is able to bring the 'history' effect to the sub-grid scales compared to an algebraic model (e.g. the Smagorinsky model) [12]. These factors are especially important in High-Re flows when the simulation is carried out with relatively course grid resolution.

The energy equation for the gas phase is included in the solution whereas the dispersed phase temperature is not taken into account. The computational mesh uses fully hexahedral cells within the spray volume having a uniform cell spacing of *dz*=0.25mm in all directions. The total amount of cells is close to 3.6 million. The mesh is shown in the Fig. 1. The dispersed phase volume fraction nor the direct coupling to the carrier phase in Eq. (1) are not taken into account.

The spatial discretization is done with central differencing and for the time integration a second order accurate three-time level method is used with constant time step size of 1µs. The flow solver used is Star-CD version 4.16.

Spray model

Lagrangian particle tracking (LPT) is used for the modelling of the dispersed phase. It is assumed that at the nozzle hole exit there may exist a short intact liquid column. Therefore, modelling of droplets is started a few millimetres downstream from the geometrical nozzle hole exit at $z \sim 6d_n$.

At $z \sim 6d_n$ it is expected that the droplet sizes are generally much smaller than at the nozzle hole exit due to fast atomization of the liquid. This assumption is based on experimental observations made e.g. in [13] where only a few millimetres from the nozzle hole turbulent flow structures and small droplets could be seen. The requirement for droplets to follow local flow field structures is that the droplet Stokes number $\mathrm{St}=\tau_p/\tau_f$ must be small ($\mathrm{St} \ll 1$). The droplet time scale is calculated from $\tau_p = \rho_d d^2 / 18 \rho_g \nu_g$,where d is the droplet diameter, and the characteristic flow time scale is calculated according to $\tau_f = l/u$,where l is the characteristic length and u is the characteristic velocity. In the following, it is shown that at $z \sim 6d_n$, there must be relatively large amount of small droplets $d \ll \mathrm{d_n}$. The condition of $\mathrm{St} \ll 1$ means that $d \ll \sqrt{\tau_f 18 \nu_g \frac{\rho_g}{\rho_d}}$. By using realistic values for this condition (l=2mm, u=200m/s, and $\rho_g/\rho_d = 0.046$), it can be seen that there must be large amount of droplets smaller than $\mathrm{d} \ll 11$µm. Consequently, in the current study the maximum droplet diameter few millimetres from the nozzle hole is restricted to $1/3\mathrm{d_n}$. At this location, droplets are distributed within a cylindrical volume that has a diameter of $3d_n$ and length of $z=dz/2$. The distribution is realized with the box-sampling method using the power-law distribution

$$g(d) = \frac{n+1}{n} \left(\frac{d}{d_n} \right)^n \quad (2)$$

In Eq. (2), the exponent n has the value of n = -3.0 in order to have relatively high probability for small droplets. As a result, the average Sauter mean diameter (SMD) at the location of droplet origin is about 25µm.

Since droplet breakup is important close to the nozzle, the Wave breakup model is used [14]. The Wave model gives the rate of change of droplet diameter d as $\frac{d\,d}{dt} = -\frac{(d - d_{stable})}{\tau_b}$. According to the regime of breakup, the characteristic breakup time τ_b is

$$\tau_b = \frac{c_{b1} \rho_d^{1/2} d^{3/2}}{4 \sigma_d^{1/2}} \quad (3)$$

for the bag breakup, and for the stripping breakup it is

$$\tau_b = \frac{c_{b2}}{2}\left(\frac{\rho_d}{\rho_g}\right)^{1/2}\frac{d}{|u-u_d|} \quad (4)$$

In the Eqs. (3) and (4) the coefficients c_{b1} and c_{b2} have been given values 20 and 80, respectively. These values are higher than typically used in RANS simulations mainly for two reasons. First, the droplet sizes given close to the nozzle are much smaller than the nozzle diameter. For the bag breakup regime in the Eq. (3), the characteristic breakup time scales as $\tau_b \sim d^{3/2}$ indicating that if droplet diameter is reduced to 1/3d, the resulting time scale is ~1/5 of the original value. For the stripping breakup regime in the Eq. (4), the time scale – droplet diameter relationship is linear. Accordingly, if droplet size is to remain at measured values after the breakup process, an increase in the values of the coefficients is needed. The second reason for the higher coefficients is that no droplet interaction model is used. Typically, droplet interaction modelling increases the average droplet sizes due to coalescence effects. A droplet dispersion model is used according to [15].

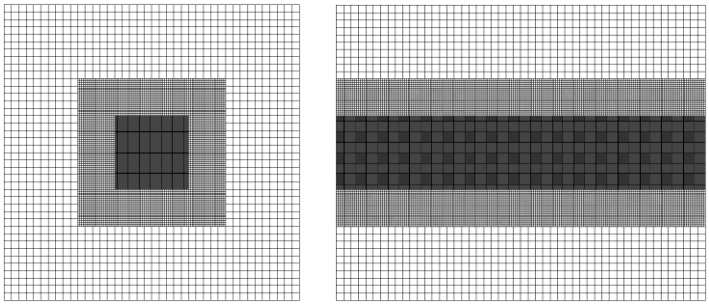

Figure 1. The computational mesh, a) nozzle is located at the centre of the dense part, b) side view from the middle of the mesh showing the dense part that has cell dimension of 0.25mm in all directions. Geometric mesh dimensions are 80 mm x 80mm x 100mm.

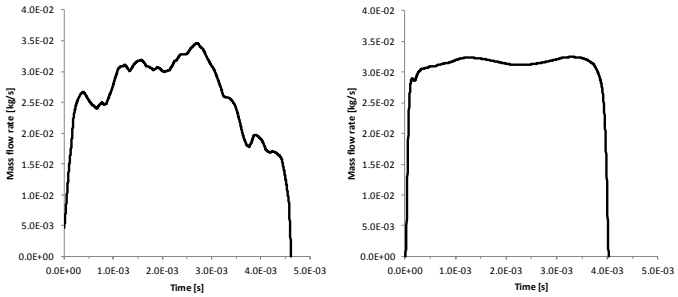

Figure 2. Simulated mass flow rate curves used as a boundary condition in the LES simulations. A) Gas density is 39 kg/m3 and injection pressure 700bar, experimental conditions from [6]. B) Gas density is 115 kg/m^3 and injection pressure 1000bar, experimental conditions as detailed in the current study.

The fuel mass flow rate curves needed as boundary conditions for the LES simulations are shown in the Fig. 2 for the 39 kg/m^3 and for the 115 kg/m^3 density cases. The calculation of the mass flow rate in the 39 kg/m^3 case has been reported in [6] where an in-house code was used to calculate the profile. On the other hand, the 115 kg/m^3 density case mass flow rate has been calculated with GT-Fuel and the model details are reported in [16]. The total mass injected in the 39 kg/m^3 gas density case is 0.119 g over the whole injection and 0.123 g in the 115 kg/m^3 gas density case. The calculated velocity at the nozzle hole exit is used as a boundary condition at $z=6d_n$. This is based on the assumption that up to $z=6d_n$ the liquid volume fraction is relatively high leading to reduced momentum transfer between the gas and the liquid phase, and hence the velocity reduction is supposedly small. The number of computational parcels used up to the simulation time of 1.7ms is about 217'000. The initial whole spray opening angle in both gas density cases was set to 24 degrees.

Results and Discussion

Figure 3 shows LES fuel sprays at different times in the gas density of 39 kg/m^3 and 115 kg/m^3. The higher gas density sprays have lower tip penetration than the lower gas density sprays. Additionally, several features can be distinguished from the sprays which can be seen in experimental fuel sprays. These include local turbulent structures, droplet clusters and droplet voids, and non-symmetric structures. Furthermore, the higher gas density of 115 kg/m^3 means that the droplet St number is lower compared to the lower density case. This is seen in the higher density sprays as very good mixing of droplets without accumulation of droplets to the central spray region. This latter phenomena is seen in the lower density sprays where large droplets (St>>1) are initially concentrated to the middle of the spray.

Figure 4 shows the q-isosurface calculated from the second invariant of the velocity gradient as $q = -\frac{1}{2}\left(\frac{\partial u_i}{\partial x_j}\frac{\partial u_j}{\partial x_i}\right)$. The q-isosurface shows the small scale structures within the sprays. The black and white colour variation is due to pressure oscillations. It is seen that LES is capable of capturing small scale structures within the sprays such as vortex tubes. Additionally, it is seen that the size of the small scale structures is increasing towards the nozzle.

In order to further analyze the spray induced turbulence field, the resolved turbulent kinetic energy was calculated from $k_{res} = 0.5(\langle u_i u_i\rangle - \langle u_i\rangle^2)$ (that can be deduced from $k_{res} = 0.5\langle\langle u_i\rangle - u_i\rangle^2$) where $\langle\ \rangle$ means time averaging. The subgrid scale turbulent kinetic energy k_{sgs} is taken from its solution in Eq. (1). Figure 5 shows the portion of k_{sgs} from k_{sgs}+k_{res} calculated from the velocity data 59mm from the nozzle at the centre of the spray axis in one cell. In the 115 kg/m^3 density case the data has been obtained 40mm from the nozzle at the spray axis. The average portion of k_{sgs} between 0.6ms – 1.7ms is about 11%.

In order to have a deeper understanding of the turbulence generation, the spray-induced volume was used to average k_{sgs} and k_{res}. Criteria used for the spray-induced volume was velocity magnitude higher than 5 m/s. On the right-hand side of the Fig. 5 is shown both the volume and time averaged portion of k_{sgs}. At maximum k_{sgs} is about 19% from the total turbulent kinetic energy defined as k_{tot}=k_{sgs}+k_{res}. Consequently, the portion of the resolved part of the turbulence is between ~80-90%. In good quality LES the portion of k_{sgs} should be relatively low so that the subgrid scale model's effect to the result is small. Additionally, it should be mentioned that k_{tot} should also include the effect from the numerical model's discretization error that act as numerical diffusion and participates to the turbulent diffusion process.

The left-hand side of Figure 6 shows the spectra of radial velocity component in a cell 59mm from the nozzle at the spray centreline in the 39 kg/m^3 gas density case taken between t = 0.6 - 1.6ms using the Fourier Transform. It can be seen from the spectra that the LES resolves a range of temporal frequencies which is necessary for it to be dynamically relevant. Furthermore, it can be noted that energy is not significantly accumulated at the smallest scales which indicates that the algorithm is dissipative enough. On the right-hand side of the Fig. 6 is shown the spray-induced volume evolution in the 39 kg/m^3 case. Assuming that the spray volume evolves like a cone, and using the Hiroyasu [17] spray penetration correlation $s \sim t^{1/2}$, it can be shown that the spray volume evolves as $V_s \sim t^{3/2}$ [18]. At early times, the spray penetration according to Hiroyasu is $s \sim t$ which results into $V_s \sim t^3$. It is seen that the LES spray volume evolves nicely according to the theoretical volume evolution.

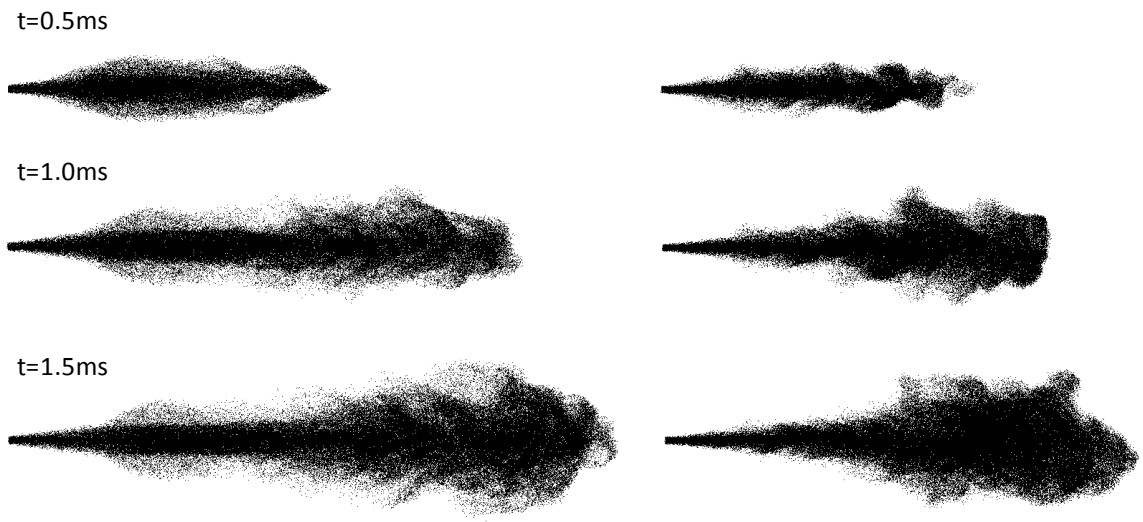

Figure 3. Fuel sprays at different times. Left: gas density is 39 kg/m^3. Right: gas density is 115 kg/m^3.

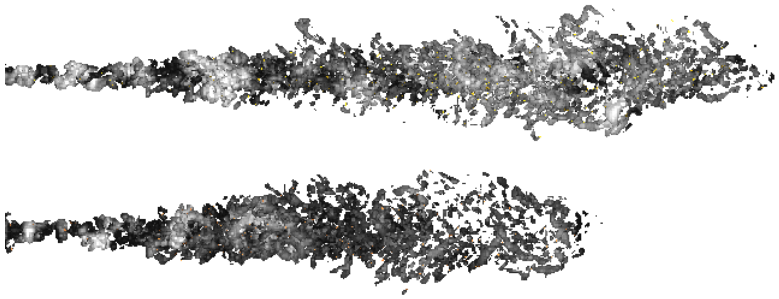

Figure 4. Q-isosurfaces from time t=1.0ms. Top: gas density is 39 kg/m^3. Bottom: gas density is 115 kg/m^3.

Figure 7 shows the experimental and computational spray penetrations. The LES result is taken as the penetration of 98% cumulative mass. The general trend is that at early times the prediction agrees well with the measured data but at later times the LES overpredicts the penetration. In general, there are several factors affecting the spray tip penetration. These include the injected mass flow rate, injection velocity, mesh density, nozzle diameter, and droplet breakup rate. In the present paper we use the Wave breakup model [14]. One of the disadvantages of the model is the non-linear coupling between the breakup model and e.g. momentum source which results in sensitivity to near nozzle velocities for instance. Further improvement and more control of the near nozzle modeling has been considered in the previous work by Vuorinen et al. [19] who proposed a framework for fully controlling e.g. the breakup length using a particle laden jet problem. Nevertheless, it is believed that the main reason for the too long penetration in the current study is related to the momentum transfer between droplets and the gas phase. As the currently used mesh is not very dense (0.25mm), the spreading of the spray induced momentum is not effective enough. This also leads to too low turbulence production near the nozzle. This can also be seen in the left-hand side of the Fig. 3 where higher turbulent fluctuations can only be seen further away from the nozzle. In some studies [8, 9] the problem with the penetration has been dealt with by increasing the turbulent viscosity. This solution has the drawback that then the LES sprays start to resemble increasingly averaged RANS sprays and is therefore not chosen in the current study.

The left-hand side of Fig. 8 shows the experimental and computational droplet Sauter mean diameter (SMD) with different radial distances from the spray axis. The LES solution was obtained from a ring-like volume where the inner diameter was 2 mm and the outer diameter 2 mm from the nominal radial distance. The axial length of the volume is 6 mm. The result was taken as the average SMD over the fully developed spray time between 1.0-1.7ms. It is seen that the LES solution is in accordance with the experimental data. LES is also able to predict some of the trend seen in the SMD versus radial distance, i.e. droplet sizes are increasing towards the edge of the spray. No experimental droplet size data is available from the 115 kg/m^3 gas density case. However, in this case the LES solution gave slightly smaller droplet sizes 60mm from the nozzle compared to the 39 kg/m^3 gas density case. The right-hand side of the Fig. 8 shows the half spray opening angle. The LES solution is obtained from 99.9% cumulative radial mass penetration. The result is taken as the average over fully developed spray time between 1.0-1.7ms. In the lower gas density case, LES somewhat underestimates the spray opening angle whereas the prediction is rather good in the higher density case.

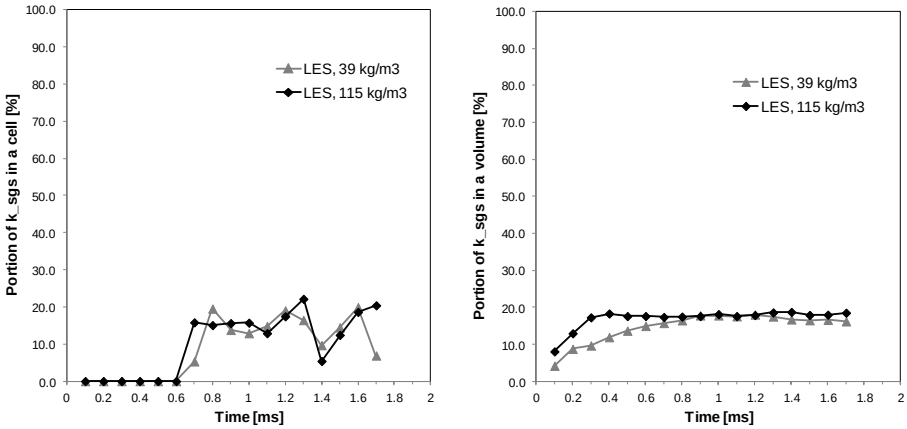

Figure 5. Left: Portion of the k_{sgs} from k_{sgs} + k_{res} in a cell 59mm from the nozzle. Right: Portion of the k_{sgs} from k_{sgs} + k_{res} in a spray-defined volume where velocity magnitude is higher than 5 m/s.

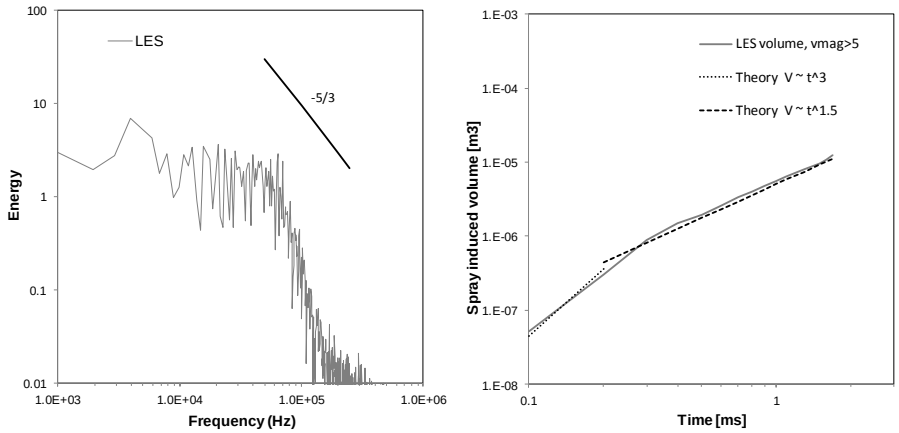

Figure 6. Left: spectra of radial velocity component 59mm from the nozzle at the spray axis. Right: spray volume evolution as a function of time compared to theory.

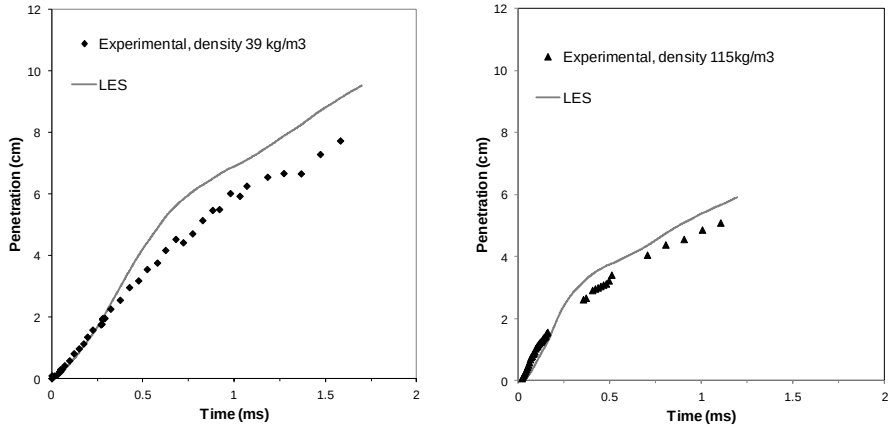

Figure 7. Left: experimental and computational spray penetration, gas density is 39 kg/m^3. Right: experimental and computational spray penetration, gas density is 115 kg/m^3

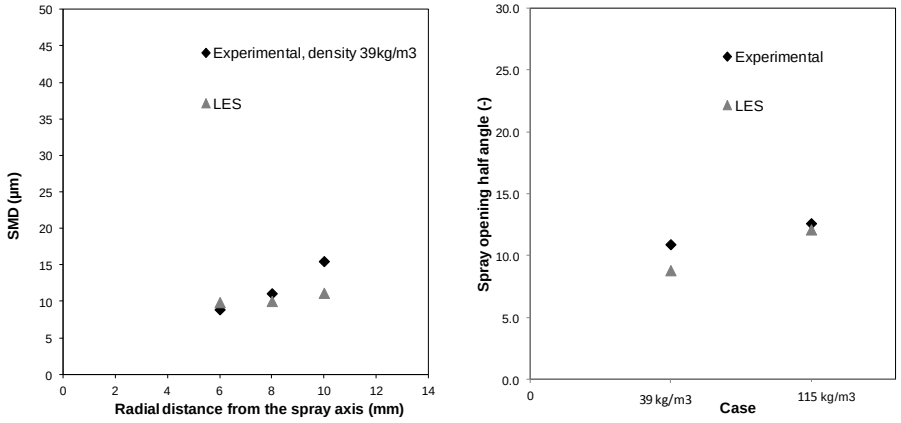

Figure 8. Left: Sauter mean diameter (SMD) of droplets 60mm from the nozzle at different radial distances from the spray axis. Gas density is 39 kg/m^3. Right: Half spray opening angle.

Conclusions

LES simulations and experiments have been carried out at two gas densities, 39 kg/m^3, and in very high gas density of 115 kg/m^3. It is observed that:

- The computed sprays in both 39 kg/m^3 gas density and in very high 115 kg/m^3 gas density have many realistic features that resemble those observed in experimental sprays. These include local turbulent structures, droplet clusters (preferential concentrations), voids, and non-symmetric features.

- LES was able to resolve large spectrum of frequencies and small scale structures which is necessary for a LES model to work properly.
- The production of turbulence was analyzed on cell basis and on a spray-induced volume basis. It was observed that the portion of the resolved scales was relatively high indicating good quality LES.
- The global parameters such as droplet sizes and opening angles were relatively well captured but the trend in the predicted spray penetration is too long. The main reason for this is in the momentum coupling between the gas phase and the dispersed phase. The mesh used in the current study is not fine enough leading to somewhat insufficient momentum spreading and turbulence production close to the nozzle. The calculated velocity boundary condition at the nozzle hole (z=0) is given as such at $z=6d_n$ assuming negligible velocity decrease during the distance of $6d_n$. This is because up to $z=6d_n$ the liquid volume fraction is high leading to reduced momentum transfer between the phases.

Acknowledgements

The authors wish to thank the Finnish Funding Agency of Technology and Innovation (Tekes) and the Cleen SHOK project Future Combustion Engine Power Plant (FCEP) for the financial support.

References

[1] J. Naber and D. Siebers, Effects of gas density and vaporization on penetration and dispersion of diesel sprays, SAE Technical paper 960034, 1996.

[2] O. Kaario, M. Imperato, A. Tilli, K. Lehto, O. Ranta, E. Antila, A. Elonheimo, T. Sarjovaara, M. Nuutinen, M. Larmi, T. Rönnskog, S. Pisilä, J. Tiainen, I. Kallio, and H. Rinta-Torala, The Design of a New Generation Medium-Speed Research Engine, Cimac, Bergen, 2010.

[3] Kaario, O., Nuutinen, M., Lehto, K., and Larmi, M., Real gas effects in high-pressure engine environment, Journal of engines, SAE International, Vol. 3, 2010-01-0627, pp. 546-555, 2010.

[4] D. Siebers, Scaling liquid-phase fuel penetration in diesel sprays based on mixing-limited vaporization, SAE Technical paper 1999-01-0528, 1999.

[5] Hiroyasu, H. and Arai, M., Structure of fuel sprays in diesel engines, Transactions of SAE, Vol. 99, Sect. 3, pp. 1050-1061, 1990.

[6] M. Larmi, P. Rantanen, J. Tiainen, J. Kiijärvi, F. Tanner, and K. Stalsberg-Zarling, Simulation of non-evaporating diesel sprays and verification with experimental data, SAE Technical paper 2002-01-0946, 2002.

[7] T. Hori, J. Senda, T. Kuge, and H. Fujimoto, Large eddy simulation of non-evaporating and evaporative diesel spray in constant volume vessel by use of KIVALES, SAE Technical paper 2006-01-3334, 2006.

[8] N. Bharadwaj and C. Rutland, A large-eddy simulation study of sub-grid two-phase interaction in particle-laden flows and diesel engine sprays, Atomization and Sprays, Vol. 20, Issue 8, pp. 673-695, 2010.

[9] G. Yejung, Large eddy simulation of dispersed multiphase flow, Phd thesis, Michigan Technological University, USA, 2012.

[10] V. Vuorinen, H. Hillamo, O. Kaario, M. Larmi, and L. Fuchs, Large-eddy simulation of droplet stokes number effects on turbulent spray shape, Atomization and Sprays, Vol. 20, Issue 2, pp. 93-114, 2010.

[11] K. Sone and S. Menon, Effect of Subgrid Modeling on the In-Cylinder Unsteady Mixing Process in a Direct Injection Engine, J. Eng. Gas Turb. Power, Vol. 125, pp. 435-443, 2003.

[12] M. M. Gibson, and B. E. Launder, Ground effects on pressure fluctuations in the atmospheric boundary layer, J. Fluid Mech., 86 (3), 491, 1978.

[13] H. Hillamo, T. Sarjovaara, O. Kaario, V. Vuorinen, and M. Larmi, Diesel spray visualization and shockwaves, Atomization and sprays, Vol. 20, Issue 3, pp. 177-189, 2010.

[14] R. Reitz and R. Diwakar, Structure of high-pressure fuel sprays, SAE Technical paper 870598, 1987.

[15] A.D. Gosman, and E. Ioannides, Aspects of computer simulation of liquid-fueled combustors, *AIAA, J. Energy*, **7**(6), pp. 482–490, 1983.

[16] K. Keskinen, O. Kaario, A. Tilli, T. Hulkkonen, and M. Larmi, Improving the accuracy of 1-D fuel injection modeling, SAE Technical paper 2012-01-1256, 2012.

[17] H. Hiroyasu, T. Kadota, and M. Arai, Supplementary comments: Fuel spray characterization in diesel engines, James N. Mattavi, and Charles A. Amann. (eds.), Combustion modeling in reciprocating engines, pp. 369-408, 1980.

[18] V. Vuorinen, H. Hillamo, O. Kaario, M. Nuutinen, M. Larmi, and L. Fuchs, Large-Eddy Simulation of Droplet Stokes Number Effects on Mixture Quality in Fuel Sprays, Atomization and Sprays, Vol. 20, Issue 5, s. 435-451, 2010.

[19] V. Vuorinen, H. Hillamo, O. Kaario, M. Nuutinen, M. Larmi, and L. Fuchs, Effect of Droplet Size and Atomization on Spray Formation: A Priori Study Using Large-Eddy Simulation, Flow Turbulence and Combustion, Vol. 86, Numbers 3-4, pp. 533-561, 2011.